



Published in final edited form as:

ACS Chem Biol. 2010 March 19; 5(3): 333–342. doi:10.1021/cb900267j.

Replacing Mn²⁺ with Co²⁺ in Human Arginase I Enhances Cytotoxicity Towards L-Arginine Auxotrophic Cancer Cell Lines

Everett M. Stone^a, Evan S. Glazer^b, Lynne Chantranupong^a, Paul Cherukuri^b, Robert M. Breece^c, David L. Tierney^c, Steven A. Curley^b, Brent L. Iverson^{d,e}, and George Georgiou^{a,d,*}

^aDepartments of Chemical Engineering, Biomedical Engineering, Molecular Genetics and Microbiology, University of Texas, Austin, TX 78712

^bDepartment of Surgical Oncology, University of Texas, M. D. Anderson Cancer Center, Houston, TX 77030

^cDept. of Chemistry and Biochemistry, Miami University, Oxford, OH 45056.

^dInstitute for Cell and Institute for Molecular and Cell Biology, University of Texas, Austin, TX 78712

^eDepartment of Chemistry & Biochemistry, University of Texas, Austin, TX 78712

Abstract

Replacing the two Mn²⁺ ions normally present in human Arginase I with Co²⁺ resulted in a significantly lowered K_M value without a concomitant reduction in k_{cat} . In addition, the pH dependence of the reaction was shifted from a pK_a of 8.5 to a pK_a of 7.5. The combination of these effects lead to a 10-fold increase in overall catalytic activity (k_{cat}/K_M) at pH 7.4, close to the pH of human serum. Just as important for therapeutic applications, Co²⁺ substitution lead to significantly increased serum stability of the enzyme. Our data can be explained by direct coordination of L-Arg to one of the Co²⁺ ions during reaction, consistent with previously reported model studies. *In vitro* cytotoxicity experiments verified that the Co²⁺ substituted human Arg I displays an approximately 12-15-fold lower IC₅₀ value for the killing of human hepatocellular carcinoma and melanoma cell lines, and thus constitutes a promising new candidate for the treatment of L-Arg auxotrophic tumors.

Keywords

Arginase; Cancer; Cobalt; Therapeutic; Hepatocellular Carcinoma; Melanoma; Enzyme Therapy

There is clearly a need for new or improved therapies for cancers such as hepatocellular carcinomas (HCCs) and melanomas that are refractile to currently used chemotherapy. Fortunately, some malignancies have underlying metabolic deficiencies that provide a unique chemotherapeutic opportunity. Many hepatocellular, prostate or renal carcinomas as well as metastatic melanomas have an impaired urea cycle and thus are auxotrophic for the non-essential amino acid L-Arginine (L-Arg), experiencing cell cycle arrest and apoptosis in its absence. Clinical trials with the L-Arg degrading enzyme arginine deiminase (ADI) from

*Address correspondence to: George Georgiou, Ph.D., 1 University Station, C0800 Austin, Texas 78712-1084, Phone: (512) 471-6975, Fax: (512) 471-7963, gg@che.utexas.edu.

BRIEFS (WORD Style "BH_Briefs"). If you are submitting your paper to a journal that requires a brief, provide a one-sentence synopsis for inclusion in the Table of Contents.

SUPPORTING INFORMATION AVAILABLE

One figure of an SDS-PAGE gel showing purified hArgI. One figure of best fits to Co-hArgI EXAFS and one table of best fit values to Co-hArgI EXAFS. This material is available free of charge via the Internet at <http://pubs.acs.org>.

Mycoplasma arginii, have been quite effective. Unfortunately, the bacterial origin of ADI results in adverse immune response after repeated administration, a major liability for extended treatment (1). L-Arg depletion therapy with the human, Mn²⁺-dependent enzyme Arginase I (hArgI), has also shown promise for cancer treatment, but has drawbacks that limit its usefulness as a drug candidate.

In contrast to constructing an optimized therapeutic enzyme by the numerous clever protein engineering techniques involving molecular biology used by this lab and others(2-6), we found that thinking about basic chemical principles was invaluable in identifying a derivative of hArgI with increased therapeutic potential. The enzyme hArgI contains a di-nuclear Mn²⁺ cofactor in its active site, which is thought to produce a metal-bound hydroxide from water in preparation for attack on the guanidinium carbon of L-Arg. Subsequent hydrolysis gives urea and L-Ornithine (L-Orn) The Mn-hArgI-catalyzed formation of a hydroxide molecule is strongly pH dependent, resulting in an enzyme with an alkaline pH optimum (~9.5)(7) and only fractional activity at physiological pH (~7.4). We reasoned that reducing the pK_a of the metal-activated water in hArgI should enhance activity at physiological pH values and result in a more effective therapeutic.

Several lines of evidence suggested that Co²⁺ would be a good choice to increase hArgI activity at physiological pH. First, the pK_a of the Co²⁺ hexaquo-cation (8.9-9.7)(8,9) is known to be about 1 pH unit lower than that of Mn²⁺ hexaquo-cation (10.4-10.6)(8-10). Second, bovine carboxypeptidase A with Mn²⁺ as a cofactor has an acidic limb kinetic pK_a of 6.4, which Co²⁺ substitution drops to 5.3 (11). Similarly the metallo-β-lactamase from *B. cereus* has a pK_a of 8.4 with Mn²⁺ that is depressed to a pK_a of 6.9 with Co²⁺ as the cofactor (12). Third, an arginase from *H. pylori* has been reported that employs Co²⁺ as the catalytic metal and displays a relatively acidic pH optimum (13). Finally, He and Lippard have prepared a series of inorganic arginase model compounds and have shown that complexes of Co²⁺, but not Mn²⁺, Zn²⁺, nor Ni²⁺, could catalyze the hydrolysis of aminoguanidinium(14). Interestingly, enhanced coordination of the substrate's amino group to the Co²⁺ ion, as opposed to a simple shift in pK_a of bound water, was presumed to be a major influence on catalytic activity in this case.

Herein we report the construction, biophysical characterization, and chemical effects of Co²⁺ substituted hArgI (Co-hArgI). Co-hArgI exhibited the expected decrease in pK_a of bound water, but also a substantial decrease in K_M of the L-Arg substrate, in the K_i for the reaction product L-Orn, as well as in increase in serum stability. The combination of these effects led to an increased cytotoxicity toward hepatocellular carcinoma and melanoma cell lines.

Results and Discussion

Results

Expression and purification of hArgI—The hArgI gene, codon-optimized for expression in *E. coli*, was constructed using overlapping oligonucleotide assembly. The final construct was fused to an N-terminal His₆ purification tag with a Tobacco Etch Virus (TEV) cleavage site and was expressed from a T7 promoter. High level expression was achieved in *E. coli* BL21 cells, and following IMAC purification, yielded ~ 200 mg hArgI /L shake flask culture (95 % pure by SDS-PAGE; Figure S1).

The effect of Co²⁺ on hArgI catalytic activity at physiological pH—As a preliminary check of activity using Co²⁺ relative to Mn²⁺, *E. coli* cells expressing hArgI were grown in minimal media and 100 μM MnSO₄ or CoCl₂ was added upon induction of protein synthesis. Addition of the metal inhibited cell growth but did not prevent protein synthesis. The rate of hydrolysis of varying concentrations of L-Arg by clarified cell lysates at pH 7.4 was determined

and used to obtain apparent K_M values of 1.5 mM and 0.16 mM for Mn^{2+} and Co^{2+} , respectively. Repeating the experiment in the presence of $NiSO_4$ or $ZnCl_2$ lead to apparent K_M values of 1.8 mM and 2.0 mM, respectively.

For detailed biochemical analyses, purified hArgI, expressed in the absence of added metal, was incubated at 50 °C for 20 minutes in the presence of either $MnSO_4$ or $CoCl_2$. Following extensive dialysis, the metal content of the protein was analyzed by inductively coupled plasma mass spectroscopy (ICP-MS). Samples of hArgI incubated with $CoCl_2$ contained 2.1 ± 0.5 equivalents Co^{2+} , 0.4 ± 0.1 equivalents Fe^{2+} and no Mn^{2+} nor Zn^{2+} , while samples incubated with $MnSO_4$ contained 1.5 ± 0.2 equivalents Mn^{2+} and 0.4 ± 0.1 equivalents Fe^{2+} . As expected, neither Co^{2+} nor Zn^{2+} were detected in the latter enzyme.

Steady state kinetic analysis in 100 mM Hepes buffer, pH 7.4 at 37 °C revealed that recombinant Mn-hArgI displays a $k_{cat} = 300 \pm 12 \text{ s}^{-1}$, $K_M = 2.3 \pm 0.3 \text{ mM}$, and $k_{cat}/K_M = 129 \pm 20 \text{ mM}^{-1} \text{ s}^{-1}$ for the hydrolysis of L-Arg. Co-hArgI displayed a 12-fold lower K_M equal to $0.19 \pm 0.04 \text{ mM}$ but a comparable k_{cat} ($240 \pm 14 \text{ s}^{-1}$) resulting in a 10 fold higher $k_{cat}/K_M = 1,260 \pm 330 \text{ mM}^{-1} \text{ s}^{-1}$ at physiological pH (Figure 1).

We measured the effect of two competitive inhibitors, product L-Orn and L-Leu at pH 7.4 and pH 8.5 (Table 1). At pH 7.4 and pH 8.5 the reaction product L-Orn was found to inhibit Mn-hArgI with a $K_I = 2.4 \pm 0.1 \text{ mM}$ and $0.53 \pm 0.06 \text{ mM}$ respectively, in a comparable range to the value reported for the rat Arginase I at pH 9.0 ($K_I = 1 \text{ mM}$)(15). Under the same conditions, Co-hArgI exhibited a $K_I = 0.076 \pm 0.016 \text{ mM}$ at pH 7.4 and a $K_I = 0.064 \pm 0.009$ at pH 8.5. The inhibition constants for the competitive inhibitor L-Leu were also calculated and found to be of similar magnitude to each other with a K_I of $0.48 \pm 0.05 \text{ mM}$ for Co-hArgI and a $K_I = 0.39 \pm 0.04 \text{ mM}$ for Mn-hArgI at pH 7.4. At pH 8.5 L-Leu bound Mn-hArgI with a $K_I = 0.64 \pm 0.04 \text{ mM}$ and Co-hArgI with $K_I = 1.3 \pm 0.15 \text{ mM}$, similar to the K_I of 1 ± 0.1 reported for hArgII (16).

pH dependence of Co-hArgI and Mn-hArgI—L-Arg hydrolysis rates by Mn-hArgI are strongly pH dependent with a log k_{cat} slope of 0.5 from pH 6 to pH 8.5. This data can be fit to a one- pK_a model (equation 3) with an apparent pK_a of 8.1 ± 0.05 in good agreement with previously reported values for hArgII (16). In contrast, Co-hArgI rates show a greatly shifted pH dependence with a tentative pK_a of 5.2 ± 0.1 (There is not much data defining this part of the curve, thus is more of an estimate). For the most part the Co-hArgI rate of hydrolysis is mostly pH independent from pH 6 – 10.5 (log slope ~ 0.03) (Figure 2A). Fits to Log plots of $1/K_M$ vs. pH show a bell shaped curve for Mn-hArgI with pK_a values of 7.1 ± 0.1 and 10.7 ± 0.3 , while Co-hArgI has apparent pK_a values of 7.2 ± 0.1 and 9.7 ± 0.1 (Figure 2B). A fit of log k_{cat}/K_M vs. pH data to a two pK_a Henderson-Hasselbach model (17) resulted in a bell shaped curve with Co-hArgI having an ascending limb pK_a of 7.4 ± 0.1 and a descending limb pK_a of 10.0 ± 0.1 . The data for Mn-hArgI could also fit a bell shaped curve with an ascending limb pK_a of 8.4 ± 0.1 and a descending limb with an apparent pK_a value of 11.0 ± 0.1 (Figure 2C). Because the fitted values are less than 3.5 pH units from each other we applied Segel's method (18) to calculate corrected pK_a values of 7.5 and 9.9 for Co-hArgI and values of 8.5 and 10.9 for Mn-hArgI. (It should be noted that there is not much data defining the descending limb pK_a of Mn-hArgI and thus is more of an estimate).

X-Ray Absorption Spectroscopy—To examine the metal site structure in more detail, X-ray absorption spectra were obtained for Co-hArgI. From the crystal structures of native di- Mn^{2+} enzymes, a six-coordinate metal ion and a five-coordinate metal ion, coordinated by one N from histidine and four or five O donors per metal ion, is anticipated. The EXAFS curve fitting results (see Supplemental Table S1 and Figures S2) indicate that the di- Co^{2+} active site is less than six-coordinate, with an average of 5 donors (1 His N and 4 O) similar to what was

observed in EXAFS study of the rat ArgI di-Mn²⁺ enzyme (19). The apparent heterogeneity of the first shell is due, in large part, to interference from Co²⁺-Co²⁺ scattering. While the first coordination sphere appears largely unchanged with respect to the native Mn²⁺ enzyme, some rearrangement is indicated, as the metal-metal separation is ~0.2 Å longer in the di-Co²⁺ enzyme (3.5 ± 0.03 vs. 3.3 Å), which may have an effect on catalysis.

Enzyme Stability—The mid-point temperature (T_M) for unfolding was determined by monitoring the change in the ellipticity at 222 nm (θ_{222}) as a function of T. A fit to the data for Co-hArgI was found to yield a T_M = 74 °C (Figure 3), essentially identical to the T_M of 75 °C reported earlier for rat Mn-ArgI (20).

The stability of the enzyme in serum was also evaluated by incubating 1 μM purified enzyme in pooled human serum at 37 °C, while monitoring the rate of hydrolysis of L-Arg as a function of time. Mn-hArgI was found to display an exponential loss of activity with a t_{1/2} = 4.8 ± 0.8 hrs. In contrast Co-hArgI exhibited far greater overall serum stability with a bi-phasic loss of activity made up of an apparent first t_{1/2} = 6.1 ± 0.6 hrs and a much slower second phase with a t_{1/2} of 37 ± 3 hrs (Figure 3 inset). Dissociation of 1 of the 2 metal equivalents in Arginase results in a reduction but not a complete loss in activity (21) and may explain the bi-phasic kinetics of the Co-hArgI enzyme, with one metal rapidly lost and the 2nd metal being lost much more slowly, corresponding to their respective K_D values. This may be species specific as mutagenesis of rat ArgI metal binding residues typically leads to orders of magnitude loss in activity (22). However, support for this hypothesis was provided by the kinetics of deactivation of Co-hArgI in 100 mM HEPES, pH 7.4, at 37 °C in the presence or absence of 500 μM Co²⁺. In the presence of extra Co²⁺, monophasic sigmoidal loss of activity was observed with a t_{1/2} = 45 ± 2 hrs.

Cytotoxicity towards human cancer cell lines—The *in vitro* cytotoxicity of Mn-hArgI and Co-hArgI towards the hepatocellular carcinoma cell line, Hep3b and the melanoma cell line A375 was evaluated. The Mn-hArgI displayed an IC₅₀ of 5.0 ± 0.7 nM towards the Hep3b cell line in excellent agreement with earlier reports (23). Consistent with its markedly improved catalytic properties, Co-hArgI showed a 15-fold lower IC₅₀ equal to 0.33 ± 0.02 nM (0.012 μg/ml) (Figure 4). The *in vitro* cytotoxicity of Mn-hArgI and Co-hArgI against melanoma cell line A375 gave similar results to the HCC experiment. Against the A375 melanoma cells, Mn-hArgI displayed an IC₅₀ of 4.1 ± 0.1 nM, while Co-hArgI showed a ~13-fold increase in cytotoxicity with an IC₅₀ value of 0.32 ± 0.06 nM.

Discussion

Recombinant hArgI was successfully derivatized with Co²⁺ as confirmed by ICP-MS analysis, which indicated 2.1 ± 0.5 equivalents Co²⁺ per enzyme. EXAFS also revealed the coordination of two Co²⁺ ions that have a similar environment, but not identical, to those of the native Mn²⁺ ions in the native enzyme. The EXAFS data obtained with Co-hArgI indicated a Co²⁺-Co²⁺ separation of 3.5 ± 0.03 Å, which is 0.2 Å longer than the Mn²⁺-Mn²⁺ separation in Mn-hArgI. It is not clear at this time how these differences might influence the catalytic hydrolysis reaction mechanism, but it is evident that Co²⁺ substitution does not drastically alter the active site of hArgI.

Detailed kinetic analyses revealed that consistent with the original experimental design, Co-hArgI exhibited a pH rate profile for the hydrolysis of L-Arg that appears to represent about a 1 pH unit drop in the pK_a of a bound nucleophilic water. In general, the pH dependence of k_{cat}/K_M is indicative of ionizations in the free enzyme and the free substrate (E + S). For Mn-hArgI, the calculated ascending limb pK_a of 8.5 most likely reflects the nucleophilic water/hydroxide equilibrium, although this curve is not well-defined at high pH values. In contrast,

Co-hArgI has a well-defined bell-shaped curve of the pH dependence of k_{cat}/K_M with an apparent $\text{p}K_a$ of 7.5, one pH unit lower than Mn-hArgI. While Co^{2+} substitution was expected to depress the $\text{p}K_a$ of bound water (8-10), the full effect may be masked by a change in the rate-limiting step. The pH dependence of k_{cat} for Co-hArgI, which reflects ionizations in the enzyme-substrate complex (ES), shows that except at acidic pH values (5-6), the k_{cat} of Co-hArgI has almost no global pH dependence (log slope = 0.03), while the Mn-hArgI rate increases more than 30-fold (log slope = 0.5) over the same range, indicating that a rate-limiting step has changed.

In light of the kinetic data, it is reasonable to propose that product release has become rate-limiting for Co-hArgI. Consistent with this notion, the inhibition constant (K_i) measured for the reaction product L-Orn with Co-hArgI was 0.076 mM, about 30-fold lower than the K_i value observed for L-Orn with Mn-hArgI (K_i of 2.4 mM) at pH 7.4. At pH 8.5 Mn-hArgI binds L-Orn about 5 fold tighter ($K_i = 0.53$ mM) than at pH 7.4, which correlates to a ~ 6 fold change in the amount of Mn-hArgI bound hydroxide, and suggests that electrostatic effects play a role in ligand binding. Similarly the 2-fold increase in bound hydroxide from pH 7.4 to 8.5 with Co-hArgI is accompanied by a ~2-fold increase in L-Orn affinity. However, Co-hArgI binds L-Orn an order of magnitude more tightly at pH 8.5 than the Mn^{2+} substituted enzyme. L-Orn has a terminal amino group, and Co^{2+} ions have a significantly higher affinity for nitrogen containing ligands compared to Mn^{2+} . Therefore, the drastic change observed upon Co^{2+} substitution can be interpreted to suggest that the metal center of Co-hArgI interacts directly with L-Orn, and this interaction is responsible for a change to rate-limiting product release. Note that L-Leu, which cannot interact with the metal center, was found to bind both Co-hArgI and Mn-hArgI approximately equally at pH 7.4 and within two-fold of each other at pH 8.5.

At pH 7.4 and 37 °C, both Mn-hArgI and Co-hArgI displayed similar k_{cat} values of 300 s^{-1} and 240 s^{-1} , respectively. However, a large change was observed in K_M values. Co-hArgI displayed a K_M of 0.19 ± 0.04 mM, about 12-fold lower than the $K_M = 2.3 \pm 0.3$ mM seen for Mn-hArgI. The net result is that at pH 7.4, Co-hArgI has a catalytic efficiency, k_{cat}/K_M , that is about 10-fold higher than Mn-hArgI. It is tempting to propose that the lower K_M value seen for Co-hArgI is the result of direct interactions between a Co^{2+} ion and one of the nitrogen atoms of the arginine substrate in analogy to the proposed interaction that occurs with the L-Orn product.

A possible mechanism is shown in Scheme 1. L-Arg is proposed to bind in the active site through direct coordination to a Co^{2+} ion. In this scenario, the L-Arg is hypothesized to be deprotonated by virtue of a shift in the guanidinium $\text{p}K_a$ in the vicinity of the strong electrostatic fields of the active site metal ions. Binding of L-Arg as the tautomer shown would facilitate nucleophilic attack by coordinated hydroxide, which in concert with an acidic group to donate a proton, would lead to a tetrahedral intermediate that ultimately collapses to form urea and metal-bound L-Orn. Departure of L-Orn and loss of a proton from bound water might regenerate the resting enzyme with a coordinated hydroxide. An important feature of the proposed mechanism is that a substrate N atom coordinates to the metal ion directly, offering a possible explanation for why the presence of Co^{2+} , which is known to have a higher affinity for nitrogen ligands compared to Mn^{2+} , exhibits a dramatically lower K_M value.

Kostic and coworkers first demonstrated that Pt^{2+} terpyridine complexes could coordinate neutral guanidines through an imine nitrogen,(24) something that was thought to be related to the strong acidity of Pt^{2+} . However, in a more biologically relevant example, the elegant work of Kimura *et al.* showed that in a 1:1 Zn^{2+} (2-guanidiny)ethyl-cyclen complex, the guanidine is a good ligand to Zn^{2+} at neutral pH in an aqueous solution. They calculated that the deprotonation of guanidinium in this complex has an apparent $\text{p}K_a$ of 5.9(25). A crystal structure of an arginase from *Bacillus caldovex* with one of the Mn^{2+} ions removed, shows

substrate L-Arg coordinated to the remaining metal by a terminal amino nitrogen (PDB:3CEV) (26). However, the guanidine-metal bond is longer and more distorted than those normally found in small molecule complexes and has not been thought to contribute greatly to substrate binding(27). This may indeed be the case for the Mn^{2+} enzyme: Khangulov *et al.* proposed a Mn^{2+} coordinated terminal guanidine nitrogen for rat ArgI based on EPR studies of the competitive inhibitors L-Lys and L-Orn. Their data indicated that L-Orn did not interact with the Mn metal center but the one methylene longer L-Lys could(28). However, the K_i values for L-Lys and L-Orn vary only slightly (0.9 mM and 1 mM respectively)(15) indicating that coordination of a N ligand to Mn^{2+} does not greatly contribute to binding. Cobalt, however, has a much greater affinity for nitrogenous ligands and as the dramatically lower K_M (L-Arg) and K_i (L-Orn) values attest, is likely coordinating substrate and product ligands when substituted into the hArgI active site. Comparing the pH dependence of Mn-hArgI and Co-hArgI upon k_{cat} , which reflects ionizations in the enzyme-substrate (ES) complex, suggests that L-Arg ionization may be greatly facilitated by Co^{2+} substitution.

From a therapeutic standpoint, the lowered K_M value and the resulting increase in catalytic efficiency are very important for the overall effectiveness of Co-hArgI relative to Mn-hArgI in cancer cytotoxicity assays. Moreover, Co-hArgI also displayed a significantly enhanced lifetime in human serum compared to Mn-hArgI. Although the origins of this effect are not certain, the fact that both derivatives were found to have similar thermal stabilities may indicate that the reason for the difference in serum stability lies in the properties of the metal ions themselves. Perhaps Co-hArgI is able to retain one or both of its metal ions longer than Mn-hArgI, an idea supported by retention of catalytic activity observed in the presence of excess Co^{2+} ion.

Conclusion

Consistent with the measured k_{cat}/K_M values, we found that Co-hArgI exhibits dramatically improved cytotoxicity against human melanoma and hepatocellular carcinoma cell lines relative to the Mn-hArgI. Engineered biological therapeutics have great potential as anti-neoplastic agents. As opposed to therapeutic antibodies which have stoichiometric interactions, an enzyme therapeutic works as a catalyst and requires far less dosing. There are a number of enzyme based cancer chemotherapies either past or under current clinical evaluation, including: L-asparaginase (Elspar), ribonuclease (Ranpirnase), methionine- γ -lyase, arginine deiminase (Hepacid) and others (29-31). In fact, Co-hArgI displayed an IC_{50} on par with that of the bacterial ADI which is currently undergoing advanced clinical evaluation. The use of human arginase I variants that display better pharmacological properties represent a major step forward in terms of the ability to treat urea cycle deficient tumors. Co-hArgI is currently undergoing extensive preclinical evaluation in a mouse xenograft model of hepatocellular cancer.

Methods

Construction of Synthetic Genes

Overlapping oligonucleotides (IDT) comprising the coding sequence of a 6 \times histidine tag, a Tobacco Etch Virus (TEV) protease recognition site, and human arginase I were combined with dNTPs, buffer and DNA polymerase (Finnzymes) and allowed to react for 30 cycles of 98 °C for 10 s, 70 °C for 20 s, and 72 °C for 1 min. A 1 μ L aliquot of this mixture was then used as a template along with specific end primers (Forward '5-GATATACCATGGGTTCTTCTCACCATCATCACCACCACAGCTCTGGCG and Reverse '5-CGAATTCGGATCCTCACTTCGGTGGATTGAGATAATCAATT) in another PCR reaction to amplify the full length gene. The cleaned product (Qiagen) was digested with NcoI and BamHI, ligated into a pET28a vector (Novagen) and transformed into *E. coli* (DH5 α).

Expression and Purification of Arginase

E. coli BL21 cells harboring plasmids containing human arginase were grown in TB media containing 50 $\mu\text{g/ml}$ kanamycin at 37 °C to an OD_{600} of ~ 0.5 upon which time IPTG was added to a concentration of 0.5 mM. After an additional ~ 12 hr of incubation at 25 °C, cells were collected by centrifugation re-suspended in IMAC buffer (10 mM $\text{NaPO}_4/10$ mM imidazole/300 mM NaCl, pH 8) and lysed by a French pressure cell. The lysates were centrifuged at $14,000 \times g$ for 20 min at 4 °C, and the resulting supernatant applied to a cobalt or nickel IMAC column, washed with 10-20 column volumes of IMAC buffer, and then proteins were eluted with IMAC elution buffer (50 mM $\text{NaPO}_4/250$ mM imidazole/300 mM NaCl, pH 8). Fractions containing enzyme were then incubated with 10 mM metal (CoCl_2 or MnSO_4) for 15 min at 50-55 °C, followed by filtration through a 0.45 μm syringe filter. Using a 10,000 MWCO centrifugal filter device (Amicon), proteins were then buffer exchanged several times into a solution comprised of 100 mM HEPES, 10 % glycerol, pH 7.4. Aliquots of purified arginase enzyme were then flash frozen in liquid nitrogen and stored at -80 °C.

Divalent Metal Screening

E. coli cells expressing arginase were grown at 37 °C in minimal media to an OD_{600} of 0.8–1. Cells were collected by centrifugation re-suspended in fresh minimal media containing 0.5 mM IPTG, 100 μM of the divalent metal-salt of choice (e.g. CoCl_2 , MnSO_4 , NiCl_2 , ZnCl_2), and incubation was continued for an additional 8–12 hours at 25 °C with shaking. Cells were collected by centrifugation and lysed by French pressure cell or by using the B-PER reagent (Pierce). Cleared supernatant was used in activity assays to determine K_M values for L-Arg hydrolysis.

Metal Identity and Stoichiometry

In order to determine metal identity content and identity, Mn-hArgI (145 μM), Co-hArgI (182 μM) and associated dialysis buffers were analyzed by inductively coupled plasma mass spectrometry (ICP-MS, Department of Geological Sciences, University of Texas at Austin). The concentration of metal found in dialysis buffer was subtracted from the value obtained in the protein sample and the data were normalized by dividing by the protein concentration. To determine protein concentrations, an extinction coefficient, $\epsilon_{280} = 24,180 \text{ M}^{-1}\text{cm}^{-1}$ was calculated for hArgI based on amino acid sequence (32). All protein concentrations were determined from the A_{280} in 6 M guanidinium hydrochloride, 20 mM phosphate buffer, pH 6.5. For comparison we also calculated arginase concentration by the BCA assay (Pierce) using dilutions of BSA as a standard and found a similar value.

Kinetic Assays

We used the diacetylmonoxine (DAMO) derivitization of urea in the presence of strong acids, thiosemicarbazide, and Fe^{3+} with heating to produce a chromophore with a λ_{max} of ~ 530 nm. The dye structure is not definitively known, but the reaction is hypothesized to be a condensation of DAMO and urea/uriedo that is possibly stabilized by Fe^{3+} ions (33). The assay was shown to be linear between 0 - 300 μM urea with a lower detection limit of 1 μM . Typically reactions were performed by equilibrating 1.5 ml Eppendorf tubes containing 200 μL of substrate at 37 °C in a heat block. Reactions were started by adding 5 μL of enzyme solution and quenching with 15 μL of 12 N HCl after 30 sec. Reactions and blanks were then mixed with 800 μL of COLDER (34) and boiled for 15 min. After cooling for 10 min, the samples were transferred to cuvettes and the A_{530} nm was determined. Because L-Arg has a background absorbance at A_{530} L-Arg blanks were included for all substrate concentrations used.

Product Inhibition of hArgI

Co-hArgI was incubated with 0.25 mM L-Arg in a 100 mM HEPES buffer, pH 7.4, at 37 °C, or with 100 mM Tris buffer pH 8.5 at 37 °C with varying concentrations of L-Orn (0 - 1 mM). Mn-hArgI was incubated with 1.5 mM L-Arg in 100 mM HEPES buffer, pH 7.4, at 37 °C in the presence of 0-6 mM L-Orn. Mn-hArgI was incubated with 1 mM L-Arg in 100 mM Tris buffer, pH 8.5, at 37 °C in the presence of 0-10 mM L-Orn. Data were expressed as percent activity, plotted versus L-Orn concentration and fit to an exponential equation to determine IC₅₀ values. The K_i values were calculated using equation (1), assuming a competitive mechanism (15) and using K_M values determined under identical conditions.

$$K_i = \frac{IC_{50}}{\left(1 + \frac{[S]}{K_M}\right)} \quad (1)$$

L-Leucine Inhibition of hArgI

Co-hArgI was incubated with 0.25 mM L-Arg in a 100 mM HEPES buffer, pH 7.4, at 37 °C with varying concentrations of L-Leucine (L-Leu) (0 - 10 mM). Co-hArgI was also incubated with 1 mM L-Arg in a 100 mM Tris buffer, pH 8.5, at 37 °C with varying concentrations of L-Leucine (L-Leu) (0 - 40 mM). Mn-hArgI was incubated with 1 mM L-Arg in 100 mM HEPES buffer, pH 7.4, or in a 100 mM Tris buffer pH 8.5 at 37 °C with varying concentrations of L-Leu (0 - 10 mM). Data were expressed as percent activity, plotted versus L-Leu concentration and fit to an exponential equation to determine IC₅₀ values. The K_i values were calculated using equation (1), assuming a competitive mechanism as reported for hArgII (16) and using K_M values determined under identical conditions.

pH Rate Dependence of Manganese Arginase, Cobalt Arginase

To examine the pH rate dependence of cobalt and manganese substituted arginase, the steady-state rate constants were determined across a broad range of pH values at 37 °C. The following buffers were used: sodium acetate (pH 5-5.5), MES (pH 6-6.5), HEPES (pH 7-7.8), Tris (pH 8-9), Capso (pH 9-10.5), all at a 100 mM concentration. All enzyme reactions were performed in at least triplicate at 37 °C. Mn²⁺ or Co²⁺ substituted arginase were each assayed with a range of substrate concentrations from 30 μM to 80 mM, depending on the pH. After fitting the kinetic data to the Michaelis-Menten equation, the k_{cat}/K_M values were calculated and plotted versus pH. The resulting bell-shaped data was fit to a form of the Henderson-Hasselbach equation (2) to determine an ascending and descending limb pK_a (where $y_{obs} = k_{cat}/K_M$ at a given pH, and $y_{max} = k_{cat}/K_M$ at the pH optimum). Because fits to two pK_a values closer than 3.5 units tend to underestimate y_{max} , Segel's method (equations 4 & 5) was used to calculate corrected pK_a values for each limb of the k_{cat}/K_M profiles (18). The pH dependence of k_{cat} showed only one apparent pK_a and was fit to equation (3) where y_{obs} is the k_{cat} at a given pH, y_{max} equals the maximum rate and where y_{min} was added to allow for a non-zero plateau at low pH values.

$$\begin{aligned} & \text{Log} [y_{obs}] \\ & = \text{Log} \left[\frac{(y_{max})}{\left(1 + 10^{(pK_{a1} - pH)} + 10^{(pH - pK_{a2})}\right)} \right] \end{aligned} \quad (2)$$

$$\begin{aligned} & \text{Log} [y_{obs}] \\ & = \text{Log} \left[y_{min} + \frac{(y_{max} - y_{min})}{(1 + 10^{(pK_a - pH)})} \right] \end{aligned} \quad (3)$$

$$K_1 [H^+]_{1/2} + 2 [H^+]_{1/2} = K_1 + 4 [H^+]_{opt} \quad (4)$$

$$[H^+]_{opt} = \sqrt{K_1 K_2} \quad (5)$$

X-Ray Absorption Spectroscopy

Samples of hArgI (~ 1 mM, including 20% (v/v) glycerol added as a glassing agent) were loaded in Lucite cuvettes with 6 μ m polypropylene windows and frozen rapidly in liquid nitrogen. X-ray absorption spectra were measured at the National Synchrotron Light Source (NSLS), beamline X3B, with a Si (111) double crystal monochromator; harmonic rejection was accomplished using a Ni focusing mirror. Fluorescence excitation spectra for all samples were measured with a 13-element solid-state Ge detector array. Samples were held at ~ 15 °K in a Displex cryostat during XAS measurements. X-ray energies were calibrated by reference to the absorption spectrum of the appropriate metal foil, measured concurrently with the protein spectra. All of the data shown represent the average of 10 scans per sample. Data collection and reduction were performed according to published procedures (35) with E_0 set to 7735 eV. The Fourier-filtered EXAFS were fit to Equation 5 using the nonlinear least-squares engine of IFEFFIT that is distributed with SixPack (36). Sixpack is available free of charge from its author, Sam Webb, at <http://www-ssrl.slac.stanford.edu/~swebb/sixpack.htm>. IFEFFIT is open source software available from <http://cars9.uchicago.edu/ifeffit> (37). Fits to unfiltered data gave similar results.

$$\chi(k) = \sum \frac{N_{as} A_s(k) S_c}{k R_{as}^2} \exp(-2k^2 \sigma_{as}^2) \exp(-2R_{as}/\lambda) \sin[2k R_{as} + \phi_{as}(k)] \quad (5)$$

In Eq. 3, N_{as} is the number of scatterers within a given radius ($R_{as}, \pm \sigma_{as}$), $A_s(k)$ is the backscattering amplitude of the absorber-scatterer (as) pair, S_c is a scale factor, $\phi_{as}(k)$ is the phase shift experienced by the photoelectron, λ is the photoelectron mean free-path, and the sum is taken over all shells of scattering atoms included in the fit. Theoretical amplitude and phase functions, $A_s(k) \exp(-2R_{as}/\lambda)$ and $\phi_{as}(k)$, were calculated using FEFF v. 8.00 (38). The scale factor ($S_c = 0.74$) and ΔE_0 (-26 eV) were determined previously (35) and held fixed throughout this analysis. Fits to the current data were obtained for all reasonable integer or half-integer coordination numbers, refining only R_{as} and σ_{as}^2 for a given shell. Multiple scattering contributions from histidine ligands were approximated according to published procedures, fixing the number of imidazole ligands per metal ion at half-integral values while varying R_{as} and σ_{as}^2 for each of the four combined ms pathways (see Table S1) (35). Co-Co scattering was modeled by fitting calculated amplitude and phase functions to the experimental EXAFS of $\text{Co}_2(\text{salpn})_2$.

Circular Dichroism Spectroscopy

A 6 μM sample of Co-hArgI in a 100 mM phosphate buffer, pH 7.4 was analyzed on a Jasco J-815 CD spectrometer. The change in molar ellipticity at 222 nm (θ_{222}) was monitored from 25 – 90 °C. The fraction of denatured protein at each temperature was calculated by the ratio of $[\theta_{222}]/[\theta_{222}]_d$ where $[\theta_{222}]_d$ is the molar ellipticity of the completely unfolded protein. The resulting data was fit to a modified logistic equation to determine the thermal transition midpoint.

Serum Stability of hArgI Variants

Purified Co-hArgI or Mn-hArgI was added to pooled human serum (Innovative, Novi MI) at a concentration of 1 μM and incubated at 37 °C. At various time points, aliquots were withdrawn and tested in triplicate for their ability to hydrolyze L-Arg (1 mM). Data were plotted as observed reaction rate vs. time and fit to either a single exponential equation, or modeled to a biphasic decay model (Equation 6) to calculate $T_{1/2}$ values (Where $y = v$ at a given time, $y_{\text{max}} = v$ at time 0, $y_{\text{mid}} = v$ at end of the first loss of activity, $y_{\text{min}} = v$ at the end of the experiment, k is an exponential rate, m is a Hill slope coefficient, $T_{0.5} = \text{time } 1/2$, and $\tau = \text{time}$).

$$y = (y_{\text{max}} - y_{\text{mid}}) e^{-kt} + \frac{(y_{\text{mid}} - y_{\text{min}})}{(1 + e^{-m(T_{0.5} - t)})} + y_{\text{min}} \quad (6)$$

Cytotoxicity of Arginase Variants

In order to test the *in vitro* cytotoxicity of arginase, varying concentrations (0 – 100 nM) of Mn-ArgI, Co-ArgI, or controls were incubated with HCC (Hep 3b) cells (American Type Culture Collection) or melanoma cells (A373) in 96-well plates at a seeding density of 500 cells/well, in DMEM media supplemented with 10% fetal bovine serum. After 24 hours of incubation at 37 °C, the cells were treated with media containing arginase in triplicate at various concentrations. The treated cells were maintained at 37 °C and 5% CO₂. Cell viability was determined by the MTT assay (Sigma-Aldrich) on days 1, 3, 5, & 7 by addition of 100 μL /well of MTT (5 mg/mL), followed by incubation for 4 hours, with gentle agitation one to two times per hour. Subsequently, the solution was aspirated, and 200 μL of DMSO was added to each well. Measurements at A₅₇₀ nm were determined and the data were normalized relative to the control solution. The resulting data was fit to an exponential equation to determine an apparent IC₅₀ value.

Supplementary Material

Refer to Web version on PubMed Central for supplementary material.

Acknowledgments

This work was supported by grants from the Texas Institute for Drug and Diagnostic Development (TI-3D) and by NIH CA 139059. LC was supported by a fellowship from the Harold & Mabel Beckman Foundation.

References

- Holtsberg FW, Ensor CM, Steiner MR, Bomalaski JS, Clark MA. Poly(ethylene glycol) (PEG) conjugated arginine deiminase: effects of PEG formulations on its pharmacological properties. *J Control Release* 2002;80:259–271. [PubMed: 11943403]
- Bloom JD, Arnold FH. In the light of directed evolution: Pathways of adaptive protein evolution. *Proceedings of the National Academy of Sciences* 2009;106:9995.

3. Park, HS.; Nam, SH.; Lee, JK.; Yoon, CN.; Mannervik, B.; Benkovic, SJ.; Kim, HS. Design and evolution of new catalytic activity with an existing protein scaffold. *American Association for the Advancement of Science*; 2006. p. 535-538.
4. Moore GL, Maranas CD, Lutz S, Benkovic SJ. Predicting crossover generation in DNA shuffling. *Proceedings of the National Academy of Sciences of the United States of America* 2001;98:3226. [PubMed: 11248060]
5. Matsumura I, Rowe LA. Whole plasmid mutagenic PCR for directed protein evolution. *Biomolecular engineering* 2005;22:73–79. [PubMed: 15857786]
6. Lutz S, Patrick WM. Novel methods for directed evolution of enzymes: quality, not quantity. *Current opinion in biotechnology* 2004;15:291–297. [PubMed: 15296927]
7. Kuhn NJ, Talbot J, Ward S. pH-sensitive control of arginase by Mn (II) ions at submicromolar concentrations. *Arch Biochem Biophys* 1991;286:217–221. [PubMed: 1910285]
8. Bickmore BR, Rosso KM, Tadanier CJ, Bylaska EJ, Doud D. Bond-valence methods for pKa prediction. II. Bond-valence, electrostatic, molecular geometry, and solvation effects. *Geochimica et Cosmochimica Acta* 2006;70:4057–4071.
9. Chaberek S Jr, Courtney RC, Martell AE. Stability of Metal Chelates. II. β -Hydroxyethyliminodiacetic Acid. *J. Am. Chem. Soc* 1952;74:5057–5060.
10. Perrin DD. The hydrolysis of manganese (II) ion. *Journal of the Chemical Society (Resumed)* 1962;1962:2197–2200. 421.
11. Auld DS, Vallee BL. Kinetics of carboxypeptidase A. pH dependence of tripeptide hydrolysis catalyzed by zinc, cobalt, and manganese enzymes. *Biochemistry* 1970;9:4352–4359. [PubMed: 5472710]
12. Badarau A, Page MI. The Variation of Catalytic Efficiency of *Bacillus cereus* Metallo- $[\beta]$ -lactamase with Different Active Site Metal Ions[†]. *Biochemistry* 2006;45:10654–10666. [PubMed: 16939217]
13. McGee DJ, Zabaleta J, Viator RJ, Testerman TL, Ochoa AC, Mendz GL. Purification and characterization of *Helicobacter pylori* arginase, RocF: unique features among the arginase superfamily. *Eur J Biochem* 2004;271:1952–1962. [PubMed: 15128304]
14. He C, Lippard SJ. Aminoguanidinium Hydrolysis Effected by a Hydroxo-Bridged Dicobalt (II) Complex as a Functional Model for Arginase and Catalyzed by Mononuclear Cobalt (II) Complexes. *J. Am. Chem. Soc* 1998;120:105–113.
15. Reczkowski RS, Ash DE. Rat liver arginase: kinetic mechanism, alternate substrates, and inhibitors. *Arch Biochem Biophys* 1994;312:31–37. [PubMed: 8031143]
16. Colleluori DM, Morris SM Jr, Ash DE. Expression, purification, and characterization of human type II arginase. *Arch Biochem Biophys* 2001;389:135–143. [PubMed: 11370664]
17. Segel, IH. *Enzyme kinetics : behavior and analysis of rapid equilibrium and steady state enzyme systems*. Wiley; New York: 1975.
18. Segel, IH. *Enzyme Kinetics*. John Wiley and Sons, Inc.; New York: 1975.
19. Stemmler TL, Sossong TM Jr, Goldstein JI, Ash DE, Elgren TE, Kurtz DM Jr, Penner-Hahn JE. EXAFS Comparison of the Dimanganese Core Structures of Manganese Catalase, Arginase, and Manganese-Substituted Ribonucleotide Reductase and Hemerythrin[†]. *Biochemistry* 1997;36:9847–9858. [PubMed: 9245417]
20. Scolnick LR, Kanyo ZF, Cavalli RC, Ash DE, Christianson DW. Altering the binuclear manganese cluster of arginase diminishes thermostability and catalytic function. *Biochemistry* 1997;36:10558–10565. [PubMed: 9265637]
21. Christianson DW, Cox JD. Catalysis by metal-activated hydroxide in zinc and manganese metalloenzymes. *Annu Rev Biochem* 1999;68:33–57. [PubMed: 10872443]
22. Cama E, Emig FA, Ash DE, Christianson DW. Structural and functional importance of first-shell metal ligands in the binuclear manganese cluster of arginase I. *Biochemistry* 2003;42:7748–7758. [PubMed: 12820884]
23. Cheng PNM, Lam TL, Lam WM, Tsui SM, Cheng AWM, Lo WH, Leung YC. Pegylated recombinant human arginase (rhArg-peg5, 000mw) inhibits the in vitro and in vivo proliferation of human hepatocellular carcinoma through arginine depletion. *Cancer Research* 2007;67:309. [PubMed: 17210712]

24. Ratilla EMA, Scott BK, Moxness MS, Kostic NM. Terminal and new bridging coordination of methylguanidine, arginine, and canavanine to platinum (II). The first crystallographic study of bonding between a transition metal and a guanidine ligand. *Inorganic Chemistry* 1990;29:918–926.
25. Aoki S, Iwaida K, Hanamoto N, Shiro M, Kimura E. Guanidine is a Zn²⁺-binding ligand at neutral pH in aqueous solution. *J. Am. Chem. Soc* 2002;124:5256–5257. [PubMed: 11996552]
26. Bewley MC, Jeffrey PD, Patchett ML, Kanyo ZF, Baker EN. Crystal structures of *Bacillus caldovelox* arginase in complex with substrate and inhibitors reveal new insights into activation, inhibition and catalysis in the arginase superfamily. *Structure* 1999;7:435–448. [PubMed: 10196128]
27. Di Costanzo L, Flores LV Jr, Christianson DW. Stereochemistry of guanidine-metal interactions: Implications for L-arginine-metal interactions in protein structure and function. *Proteins: Structure, Function, and Bioinformatics* 2006;65
28. Khangulov SV, Sossong TM Jr, Ash DE, Dismukes GC. L-Arginine Binding to Liver Arginase Requires Proton Transfer to Gateway Residue His141 and Coordination of the Guanidinium Group to the Dimanganese (II, II) Center†. *Biochemistry* 1998;37:8539–8550. [PubMed: 9622506]
29. Izzo F, Marra P, Beneduce G, Castello G, Vallone P, De Rosa V, Cremona F, Ensor CM, Holtsberg FW, Bomalaski JS, Clark MA, Ng C, Curley SA. Pegylated arginine deiminase treatment of patients with unresectable hepatocellular carcinoma: results from phase I/II studies. *J Clin Oncol* 2004;22:1815–1822. [PubMed: 15143074]
30. Lee JE, Raines RT. Ribonucleases as novel chemotherapeutics: the ranpirnase example. *BioDrugs* 2008;22:53–58. [PubMed: 18215091]
31. Hu J, Cheung NKV. Methionine depletion with recombinant methioninase: In vitro and in vivo efficacy against neuroblastoma and its synergism with chemotherapeutic drugs. *International Journal of Cancer* 2009;124
32. Gill SC, von Hippel PH. Calculation of protein extinction coefficients from amino acid sequence data. *Anal Biochem* 1989;182:319–326. [PubMed: 2610349]
33. Beale RN, Croft D. A sensitive method for the colorimetric determination of urea. *J Clin Pathol* 1961;14:418–424. [PubMed: 13688207]
34. Knipp M, Vasak M. A colorimetric 96-well microtiter plate assay for the determination of enzymatically formed citrulline. *Anal Biochem* 2000;286:257–264. [PubMed: 11067748]
35. Periyannan GR, Costello AL, Tierney DL, Yang KW, Bennett B, Crowder MW. Sequential Binding of Cobalt (II) to Metallo-[beta]-lactamase CcrA†. *Biochemistry* 2006;45:1313–1320. [PubMed: 16430228]
36. Webb SM. SIXPACK: a graphical user interface for XAS analysis using IFEFFIT. *Physica Scripta* 2005;115:1011–1014.
37. Newville M. IFEFFIT: interactive XAFS analysis and FEFF fitting. *Journal of Synchrotron Radiation* 2001;8:0495.
38. Ankudinov AL, Ravel B, Rehr JJ, Conradson SD. Real-space multiple-scattering calculation and interpretation of x-ray-absorption near-edge structure. *Physical Review B* 1998;58:7565–7576.

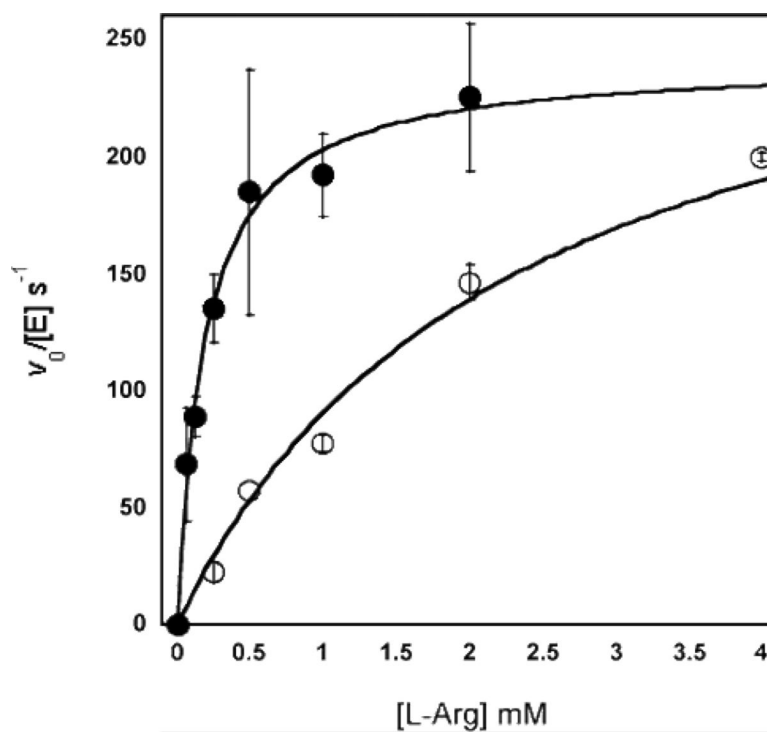


Figure 1. Comparison of steady-state kinetics of hArgI substituted with Mn or Co in a 100 mM Hepes buffer, pH 7.4, 37 C. Co-hArgI (●) had a k_{cat} of $240 \pm 14 \text{ s}^{-1}$, a K_M of $190 \pm 40 \mu\text{M}$, and k_{cat}/K_M of $1,270 \pm 330 \text{ mM}^{-1} \text{ s}^{-1}$, as compared to Mn-ArgI (○) where we found a k_{cat} of $300 \pm 12 \text{ s}^{-1}$, a K_M of $2,330 \pm 260 \mu\text{M}$, and k_{cat}/K_M of $129 \pm 20 \text{ mM}^{-1} \text{ s}^{-1}$.

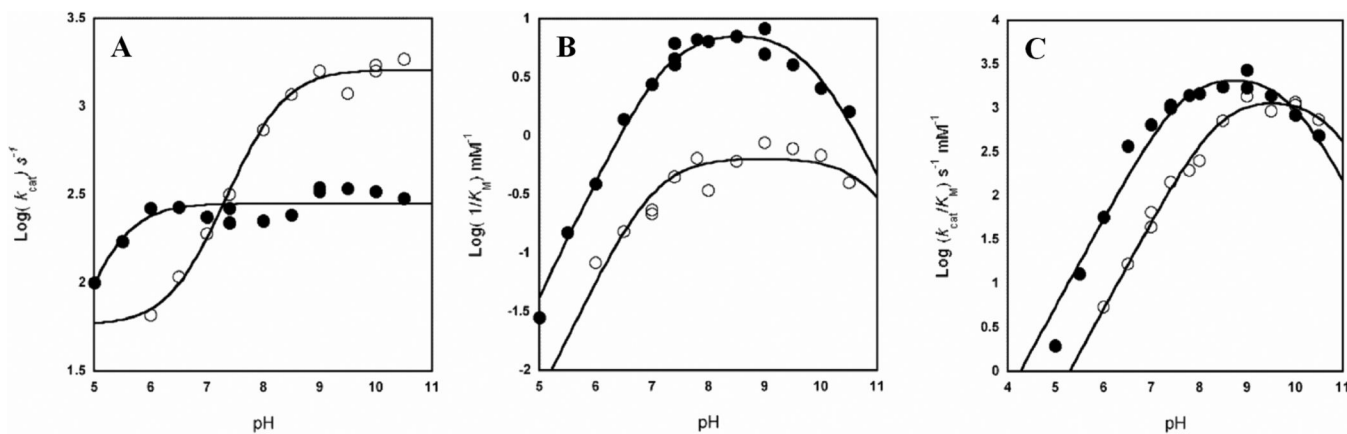


Figure 2.

Log plots of the pH dependence of Michaelis-Menten parameters for Co-hArgI (●) and Mn-ArgI (○) hydrolysis of L-Arg. **A.** The k_{cat} of Mn-hArgI (○) is dependent on pH (Log slope = 0.5 between pH 6 – 8.5). The k_{cat} of Co-hArgI (●) has a pH dependence between 5 - 6 (Log slope = 0.43) but only varies slightly with pH between pH 6 – 10.5 (Log slope = 0.03). **B.** The pH dependence of $1/K_M$ for Co-hArgI (●) is bell-shaped and has apparent pK_a values of 7.3 and 9.7. The pH dependence of $1/K_M$ for Mn-hArgI (○) is also bell-shaped and has apparent pK_a values of 7.1 and 10.7. **C.** The pH dependence of k_{cat}/K_M shows an ascending limb pK_a value of 8.5 for Mn-hArgI (○) which drops a pH unit to 7.5 for Co-hArgI (●).

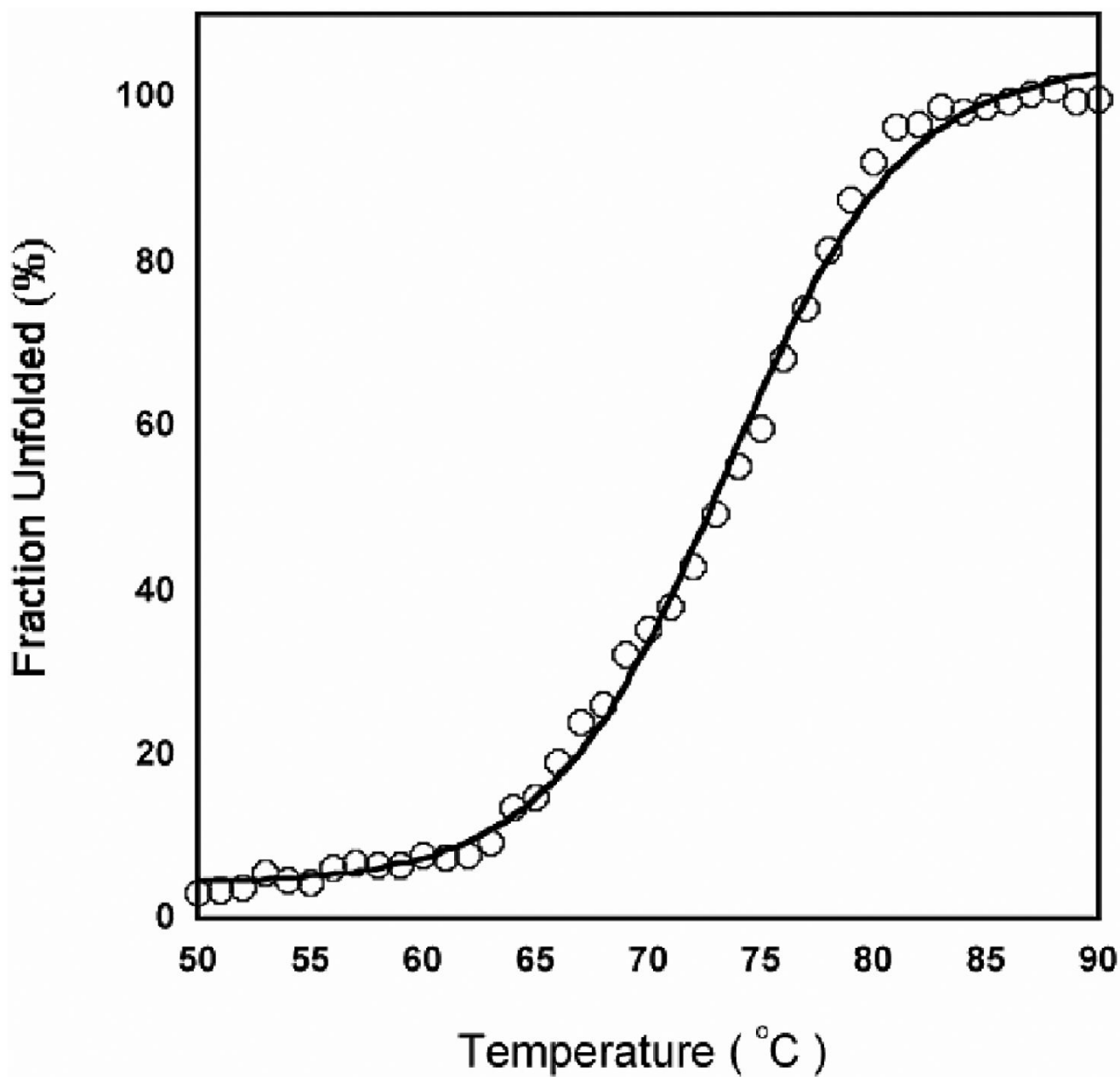


Figure 3. Thermal denaturation of Co-hArgI. A T_M of 74 °C was determined in excellent agreement with previously recorded values for rat Mn-ArgI (20).

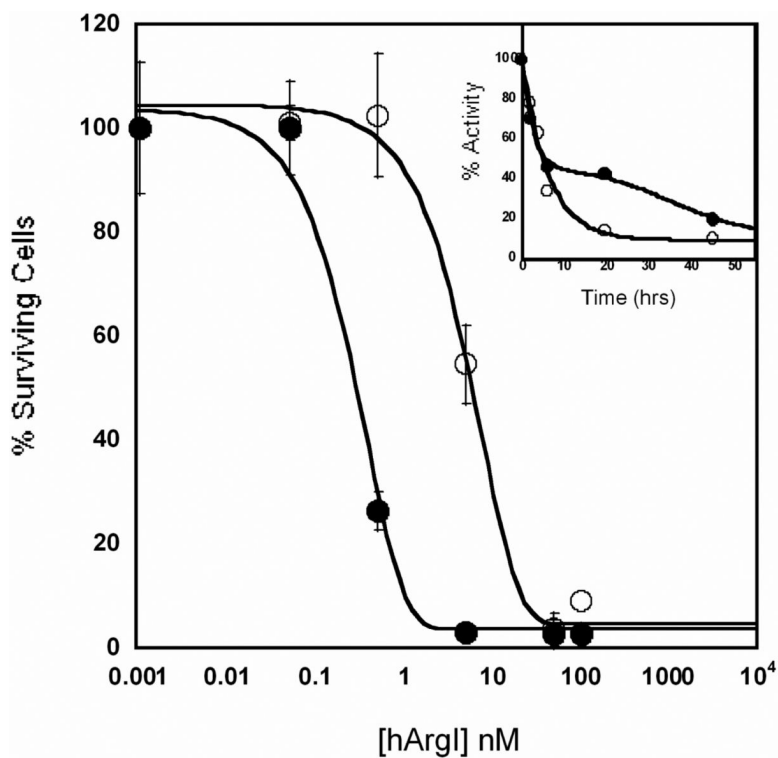
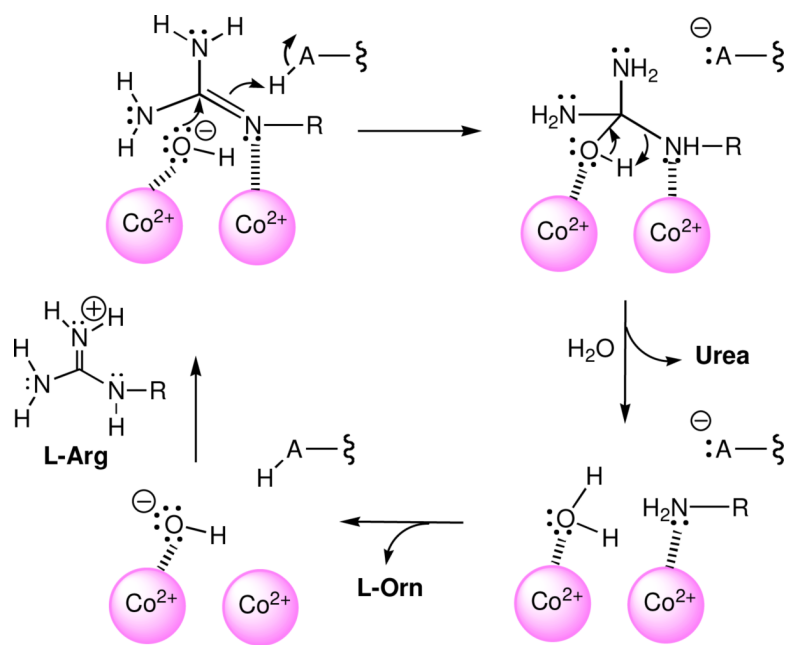


Figure 4. Representative graph of the effect hArgI on the growth Hep3b cancer cells (Day 5). Mn-hArgI (○), resulted in an apparent IC_{50} of 5 ± 0.3 nM (~ 0.18 $\mu\text{g/ml}$). Incubations with Co-hArgI (●) lead to a 15-fold increase in cytotoxicity with an apparent IC_{50} of 0.33 ± 0.02 nM (~ 0.012 $\mu\text{g/ml}$). **Inset:** Stability of Co-hArgI or Mn-hArgI (1 μM) incubated in pooled human serum at 37°C . Mn-hArgI (○) displayed an exponential loss of activity with a $T_{1/2}$ life of 4.8 ± 0.8 hrs. In contrast Co-hArgI (●) displayed a bi-phasic loss of activity with an apparent first $T_{1/2}$ of 6.1 ± 0.6 hrs followed by much longer second $T_{1/2}$ of 37 ± 3 hrs.

**Scheme 1.**

In this proposed mechanism Co-hArgI coordinates a hydroxide molecule. Upon substrate binding L-Arg is deprotonated by Co^{2+} and coordinated via an imino guanidine nitrogen. The coordinated hydroxide can then attack the guanidinium carbon and pick up a proton from a general acid. This transient tetrahedral intermediate would then collapse into product urea and L-Orn . Water could then displace L-Orn , and be ionized to hydroxide, regenerating the resting enzyme.

Table 1

Comparison of Mn-hArgI & Co-hArgI Inhibition Constants at pH 7.4 and pH 8.5.

	K_{iL-Leu} μ M	K_{iL-Orn} μ M	K_{ML-Arg} μ M	% OH-bound
Mn-hArgI (pH 7.4)	390 \pm 40	2,400 \pm 100	2,300 \pm 330	8
Mn-hArgI (pH 8.5)	640 \pm 40	530 \pm 60	1,600 \pm 140	50
Fold change	(1.6)	(4.5)	(1.4)	(6.3)
Co-hArgI (pH 7.4)	480 \pm 50	76 \pm 16	190 \pm 40	44
Co-hArgI (pH 8.5)	1,300 \pm 150	50 \pm 7	140 \pm 10	91
Fold change	(2.7)	(1.5)	(1.4)	(2.1)